CrossMark

A catalyst-free synthesis of germanium nanowires obtained by combined X-ray chemical vapour deposition of GeH$_4$ and low-temperature thermal treatment techniques

CHIARA DEMARIA[1], ALDO ARRAIS[2,*], PAOLA BENZI[1], ENRICO BOCCALERI[2], PAOLA ANTONIOTTI[1], ROBERTO RABEZZANA[1] and LORENZA OPERTI[1]

[1]Dipartimento di Chimica and NIS Centre of Excellence, Università degli Studi di Torino, via Pietro Giuria 7, 10125 Torino, Italy
[2]Dipartimento di Scienze e Innovazione Tecnologica and Centro NanoSi.S.Te.M.I., Università degli Studi del Piemonte Orientale, viale Teresa Michel 11, 15121 Alessandria, Italy

Abstract. A catalyst-free innovative synthesis, by combined X-ray chemical vapour deposition and low-temperature thermal treatments, which has not been applied since so far to the growth of germanium nanowires (Ge-NWs), produced high yields of the nanoproducts with the GeH$_4$ reactant gas. Nanowires were grown on both surfaces of a conventional deposition quartz substrate. They were featured with high purity and very large aspect ratios (ranging from 100 to 500). Products were characterized by scanning electron microscopy with energy-dispersive atomic X-ray fluorescence and transmission electron microscopies, X-ray powder diffraction diffractometry, thermogravimetric analysis with differential scanning calorimetry, vibrational infrared and Raman and ultraviolet–visible–near infrared spectroscopies. A quantitative nanowire bundles formation was observed in the lower surface of the quartz substrate positioned over a heating support, whilst spots of nanoflowers constituted by Ge-NWs emerged from a bulk amorphous germanium film matter, deposited on the upper surface of the substrate. The nanoproducts were characterized by crystalline core morphology, providing semiconductive features and optical band gap of about 0.67 eV. The possible interpretative base-growth mechanisms of the nanowires, stimulated by the concomitant application of radiant and thermal conditions with no specific added metal catalyst, are hereafter investigated and presented.

Keywords. Nanostructures; chemical vapour deposition (CVD); heat treatment; electron microscopy; powder diffraction; Raman spectroscopy and scattering.

1. Introduction

Germanium-based materials are provided with intrinsic semi-conductive features that ensure application in different technical devices, e.g., diodes [1], transistors [2], photovoltaic panels [3], laser [4], detectors [5]. In recent times, in nanotechnology context the patterned syntheses of germanium nanowires (Ge-NWs) has added geometrical and structural improvement to the opto-electronic characteristics [6], to gain a particular attention in the context of nanoscience and nanotechnology [7,8]. Since so far, Ge-NWs have been basically synthesized at laboratory scale by high-pressure solvothermal [9,10] and template-assisted electrochemical [11], laser ablation [12] and high-temperature chemical transport [13] treatments of Ge-containing chemical precursors, with different reports that presented high-quality Ge-NWs production from the chemical vapour deposition (CVD) technique of Ge gaseous precursor molecules [14–18] and H$_2$ [19], albeit in lesser abundance than for the related

carbon nanotubes scenario [20]. However, with noteworthy exceptions [12,21,22], common synthetic protocols in literature, although with different operating mechanisms, are actually based on the active catalytic cooperation of a metal nanoparticle [23–27], usually pre-deposited on the selected growth substrate [15,19,28,29], that is mainly determinant for Ge-NW formation and it is often left embedded inside the final material after reaction, as a contamination element [30,31].

In this study, an innovative catalyst-free synthesis in quantitative extents of Ge-NWs featured with high purity and quality, obtained by a combined application of CVD activated by X-ray irradiation (X-ray CVD) [32,33] and of thermal treatment technique of the deposition substrate, is reported. The X-ray radiolytic CVD technique, which has never been applied since so far to Ge-NW synthesis, provides an high amount of energy, to promote the chemical dissociation of gaseous precursors and the formation of highly reactive species (i.e., ions and radicals) [34] that enhance the deposition process on thermal-activated surfaces [35]. The nanoproducts have been grown straightforwardly from

the single monogermane (GeH_4) molecular gas precursor on common quartz substrates, without a conventional catalytic support of deposited metal nanoparticles, at low synthetic temperatures. The materials have been characterized by scanning electron microscopy (SEM) with energy-dispersive atomic X-ray fluorescence (EDAX), transmission electron microscopy (TEM), elemental analysis (CHNS-O), X-ray powder diffraction (XRPD), Thermo-gravimetric analysis with differential scanning calorimetry (TGA-DSC), vibrational infrared (IR) and Raman spectroscopy, electron ultraviolet–visible–near-infrared (UV–VIS–NIR) spectroscopy, current measurement.

2. Materials and methods

The reactor was formed by a metal vacuum chamber (1350 l volume). An heating platelet was set on the bottom of the cell, to favour the exposure through a polymer window to the ionizing beam (Gilardoni CPX-T 320 X-ray source, Italy, with a maximum energy output of 320 keV) of both the reactant gas and the thermally activated deposition substrate. The heating support was a copper disc (0.5 cm diameter) connected to heating platelet, on which the deposition substrates (quartz discs, VPQ 300) were positioned. An outer water cooling system operates. A comprehensive technical scheme of the X-ray CVD-thermal treatment hyphenated experiment is proposed in scheme 1. The reactor was positioned in contact with the X-ray beam window. The deposition substrate, connected to an heating platelet, was set on the main X-ray beam trajectory. GeH_4 was purchased by SIAD (Italy).
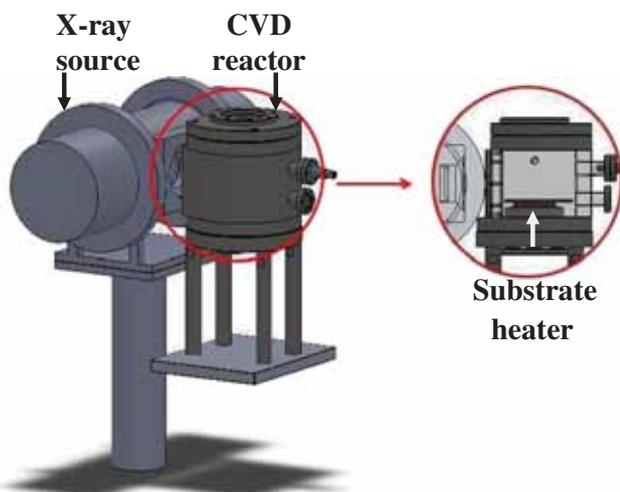
3. Experimental

Synthetically, in a typical reaction procedure, a voltage of 250 kV and a current of 10 mA were applied in the X-ray generator tube (activation X-ray energy expressed as absorbed dose rate of 5×10^3 Gy h^{-1}). GeH_4 at a starting

Scheme 1. Comprehensive technical schematic design of the X-ray CVD-thermal treatment experiment.

pressure of 700 Torr (9.2×10^4 Pa) was irradiated for 3 h, over a quartz substrate disc, heated at 300°C. After cooling at room temperature, the collected quartz specimen resulted provided with a uniform lucid and a powder wear, deposited on the higher and on the lower disc surface, respectively. Reacted solids deposited nearby on the Cu heating element were collected separately.

SEM-EDAX pictures and element X-ray fluorescence spectra were collected on two different Philips-Fey Quanta 200 scansion electron microscopy serial items. Supporting SEM-EDAX supplementary analysis was detected on a Leo VP1450-Oxford EDAX probe hyphenated set-up. TEM picture frames were collected on a Philips Fey CM10 transmission electron microscopy apparatus. XRPD measurements were executed on a Thermo 'XTRA 048 diffractometer, equipped with a 1.540562 Å Cu-emitting $K_{\alpha 1}$ X-ray radiation, supplied at 45 kV and 40 mA (scan rate 0.75 2θ min^{-1}). The measurements of the thickness of deposited products were performed with a Dektak 150 Veeco profilometer. Raman and Fourier-transformed (FT) IR vibrational measurements were performed on a Bruker Vertex 70 RAM II multimodal apparatus, with 1.064 μm NdYAG laser Raman source (with laser power in 50–75 mW range), at 4 and 2 cm^{-1} resolution for the collection of Raman and IR spectra, respectively. The composition of the solids was determined using a Thermo Electron Corporation CHNS-O analyser for the determination of the H and O content, while the Ge content was calculated as the difference. TGA-DSC analysis was performed on a Setaram SetSys 1750 Evolution thermobalance, under purity-grade (99.995%) O_2 atmosphere, in the 30–900°C thermal range, with a 5°C min^{-1} heating ramp rate. UV–VIS–NIR measurements were performed on a Perkin-Elmer Lambda 900 double-ray spectrophotometer. Conductive measurements were obtained on substrate-deposited materials with a Jandel multi purpose four-point probing system.

4. Results and discussion

The products grown on both the surfaces of the quartz substrate were examined. The materials were characterized by SEM. In figure 1a–d, bulk production of large aspect ratio (i.e., the length/diameter structural ratio), regular-shaped Ge-NW materials can be observed for deposited materials on the lower surface of the quartz disc. Lengths of NWs up to 20 μm and over were screened (with an aspect ratio of about 100 : 1, figure 1a–d). Among these NWs, there is a substantial lack of different by-product morphologies, like aggregated spheroids of amorphous hydrogenated germanium which can be obtained with X-ray CVD activation of Ge gaseous reactants [32,33]. Herein, the presented high aspect ratio morphologies resulting from the reported synthetic experimental set-up, although featured with large NW diameters, are appropriate standard results in the germanium NW scenario [6,10,11,13–15,36]. Noteworthy, with the reported experimental procedure, NWs are produced with

straightforward reaction of the GeH_4 at low synthesis temperature (300°C) [13–15]. On conventional quartz substrates, the comprehensive Ge-NW nanomaterials are experimentally obtained in bundles and noodles. In nanotechnology perspective, however, with nano-engineered deposition substrates (e.g., metal, mesoporous silica and alumina) [14,15,19,36], the vertically aligned and patterned growth of Ge-NWs with this hyphenated technique may be obtained. Multiple EDAX analyses of the Ge-NW bundles and single filaments products on both surfaces collected comprehensively the specific X-ray fluorescence emissions of germanium and of the supporting SiO_2 substrate. The possible supplementary heteroelements incorporated on the surface or inside the nanoframes were not observed. A representative EDAX analysis of a SEM-selected area containing bundles of Ge-NWs deposited on bottom surface of the quartz substrate is illustrated in figure 2. Accumulated acquisition of the X-ray fluorescence atomic spectrum supported production of high-purity Ge-NWs.

In figure 3, TEM images of the NWs provide information about their essentially regular-shaped cylindrical features, distorted by bundling and by local regions of bent NW growth (figure 3a, b). A detail of a single Ge-NW nanofilament is provided (figure 3c). In figure 3d, the correlated TEM electron diffraction pattern is depicted, which actually supports the NW core high crystallinity. The observed lattice symmetry is specific of a germanium crystal phase. Herein, the lattice parameters can be extrapolated and, within the estimated measurement errors, are coherent to literature data [14]. Noteworthy, a small yield of Ge amorphous phase is observed in the screened NWs, although different splitted electron diffraction spots (inset detail of figure 3d) can be provided by a comprehensive scenario of multi-crystalline Ge domains.

The XRPD diffraction pattern of Ge-NWs is illustrated in figure 4a. It supports these results, although with broad peaks, that can be associated to the crystalline Ge phase, which are observed at about 30, 50, and a very small one at 80 2θ (deg) [13,14]. The main peak at 30° is determined by the (111) index of the diamond crystal phase of Ge [14,37]. Noteworthy, the broader patterned peak at 50° can be actually a combination of both the (220) peak, at about 45°, and of the Ge (311) peak, at about 55° [19]. The presented diffraction item with broad peaks should not be determined by a finite size effect in NWs with diameters around 200 nm, but rather by a comprehensive low crystalline arrangement of the NW nanomaterials synthesized in X-ray stimulated
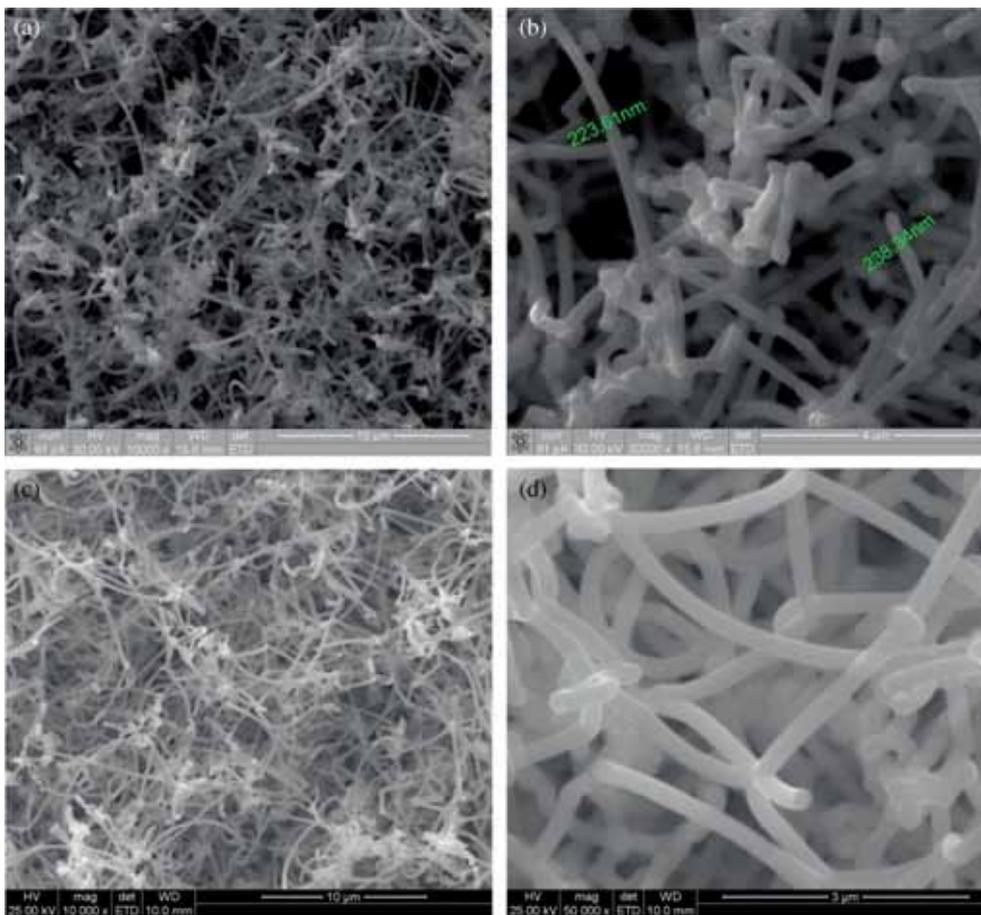

Figure 1. SEM pictures of Ge-NW products deposited on the lower surface of the quartz substrate (**a–d**). Specific diameters of NW frames are reported (**b**).

high-energy conditions. The high purity of Ge gas reactants and nanoproducts eliminates the possibility of amorphous states determined by chemical disorder [14]. In this
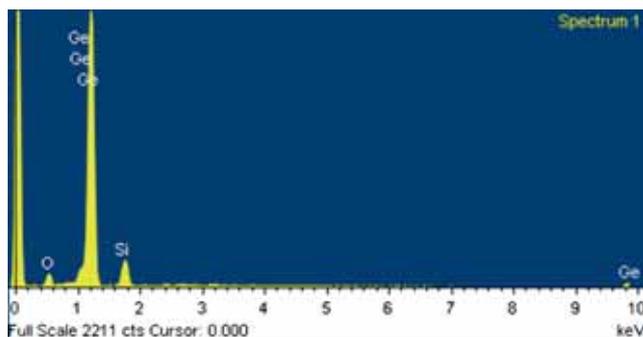

Figure 2. Standard EDAX spectrum originated from a SEM-selected scenario of Ge-NWs grown on the lower quartz substrate surface. Si and O peaks are provided by the deposition substrate.

context, a diffuse low crystallinity of Ge-NWs may derive intrinsically either from the metastable growth deposition process of highly reactive Ge species, from NW surface energy reduction, or from posterior induced peripheral strain and stress interaction with the deposition substrate [14,15,38]. Noteworthy, core–shell morphological architectures of germanium NWs, with a crystal core embedded in a less-ordered nanocrystalline or amorphous Ge-shell, have been reported, providing a broad-peak experimental XRPD diffraction pattern [14]. The deposited materials on the upper substrate surface (figure 4b) are characterized by a main amorphous morphology, as the observed peak is determined by the supporting embedded quartz substrate, by comparison with reference pattern of figure 4c. The supplementary reference XRD profile excludes the presence of the quartz substrate in the observed diffractogram of Ge-NWs.

The measurement of the deposited solid thickness, obtained with the profilometer, results of about 120 nm for
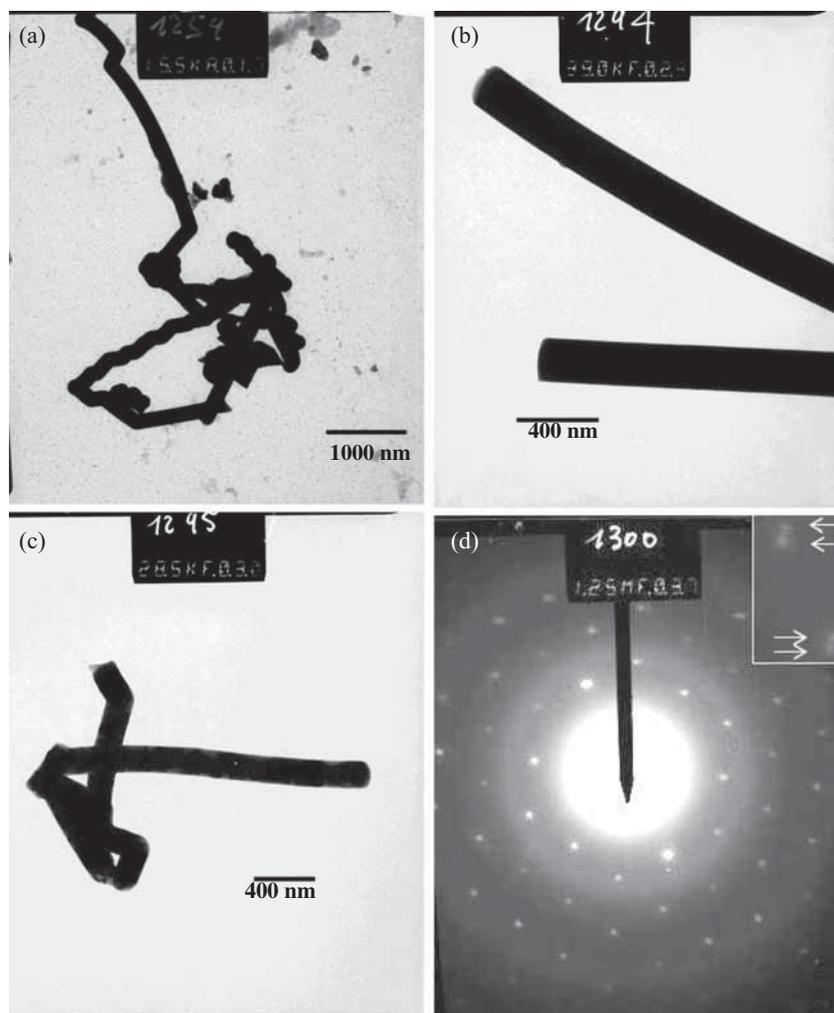

Figure 3. TEM picture of a Ge-NW bundle frame (**a**). Two separated NWs (**b**). A detail of a Ge-NW nanofilament (**c**). Convergent beam (100 keV, 1.25 mF) crystalline electron diffraction pattern of the nanofilament (**d**). In the inset, splitted electron diffraction spots can be observed.
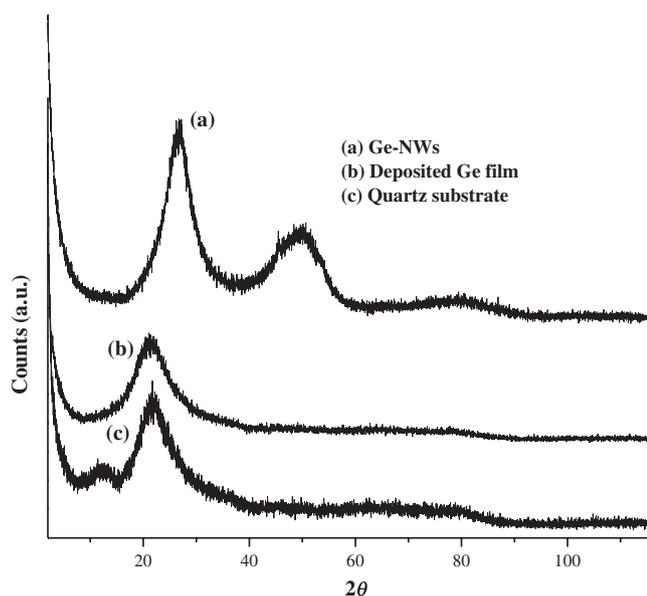
Figure 4. XRPD patterns of (**a**) Ge-NW nanoproducts, (**b**) deposited Ge film on higher substrate surface and (**c**) quartz deposition substrate.

Figure 5. Raman spectrum (1064 nm NdYAG laser source, 4 cm^{-1} resolution) of Ge-NW nanoproducts (**a**) and deposited Ge film on higher substrate surface (**b**). In the inset, IR spectra of host KBr (**c**) and Ge-NWs (**d**) are reported.

the film grown above the quartz substrate (i.e., that mainly exposed to the radiant beam), whilst the Ge-NWs layer below the substrate is about 8 μm.

Raman spectroscopy of the Ge-NWs substrate presents a broad vibrational pattern at low wavenumbers, in which three main absorptions can be observed. The result is illustrated in figure 5a. Actually, the shape of this spectral profile is generated by the overlap of five diagnostic peaks, four (at about 275, 220, 160 and 80 cm^{-1}) related to amorphous and one (centred at 300 cm^{-1}) related to crystalline vibrational solid-state germanium mode [14,32,33]. Noteworthy, the position frequency and the full-width at half-maximum (FWHM) of the transverse optical (TO) mode (at about 275 cm^{-1}) are correlated to the short-range order, whereas the ratio between the intensity of the transverse acoustic (TA) mode (at about 80 cm^{-1}) and TO mode is associated to intermediate-range order: smaller TO FWHM and I_{TA}/I_{TO} intensity ratio, together with higher wavenumber TO shift, are correlated to higher germanium crystalline order [33,39]. Experimentally, by deconvolution extrapolation, it was observed that in Ge-NWs obtained by combined techniques the TO frequency position increases and TO FWHM and I_{TA}/I_{TO} decrease with respect to the materials obtained by simple X-ray radiolysis, which is consistent with a larger structural order of the nanoproducts [33,39]. However, conformably to XRPD results, spectral profiles are broadened by a less-ordered Ge component in the NWs. The Raman spectrum of the materials deposited in the upper surface of the quartz substrate is shown in figure 5b. It presents a main amorphous state of the solids deposited in the reaction film.

FT-IR measurements of Ge-NW products (inset of figure 5, pattern d) provide a substantially silent vibrational profile;
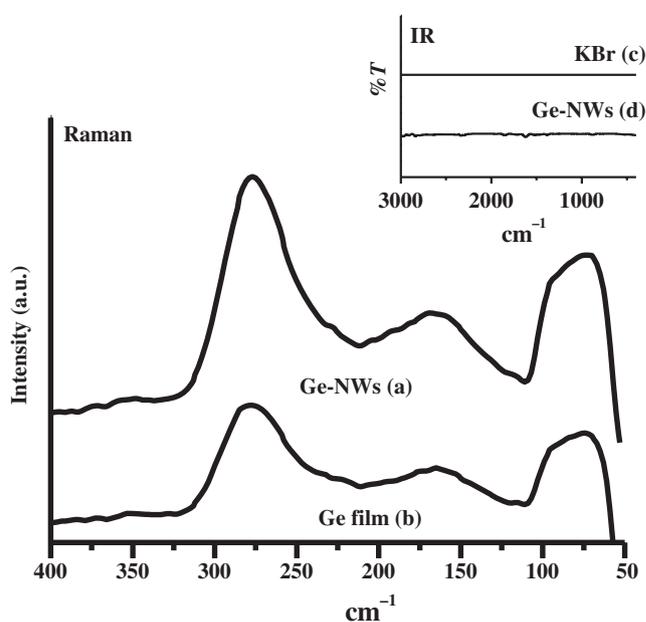
no diagnostic signals related to stretching modes of Ge–H (2200–2100 cm^{-1}) [32,33] and Ge–O (900–700 cm^{-1}) [32] groups support the high purity of the produced Ge nanomaterials.

This spectral result is strengthened by elemental analyses operated on different specimens of the bulk nanomaterial and on products formed above the deposition substrate, from which no hydrogen and oxygen contents were observed.

The TGA analysis performed under O_2 conditions (100%) at a slow heating ramp rate (5°C min^{-1}), in the 30–900°C thermal range, is illustrated in figure 6. The measurement provides a pattern that correspond to high purity of the Ge substrates. Two main oxidative processes are observed, at 620 and at 825°C, respectively, determined by germanium reaction with molecular oxygen to produce germanium oxide. Noteworthy, the weight increment after sample oxidation is quantitatively consistent with Ge oxidation to GeO_2. The supplementary DSC pattern is illustrated in figure 7. It features two coherent strong exothermal peaks, resulting patterned in the hyphenated TGA-DSC simultaneous experiment, which are set in relationship with the corresponding TGA ramp and support oxidation of the nanoframes at those temperatures. Both the linear ramp and the sharp peak pattern features of the TGA and of the DSC experiments are induced by regular-shaped morphology of the Ge-NW nanoproducts. The TGA analysis noticed the Ge-NW nanoproducts stability to oxidative processes at high temperatures. Moreover, the features of Ge-NWs over time have been explored by IR analyses on materials stored for several months under room aerobic conditions, which supported their comprehensive stability.
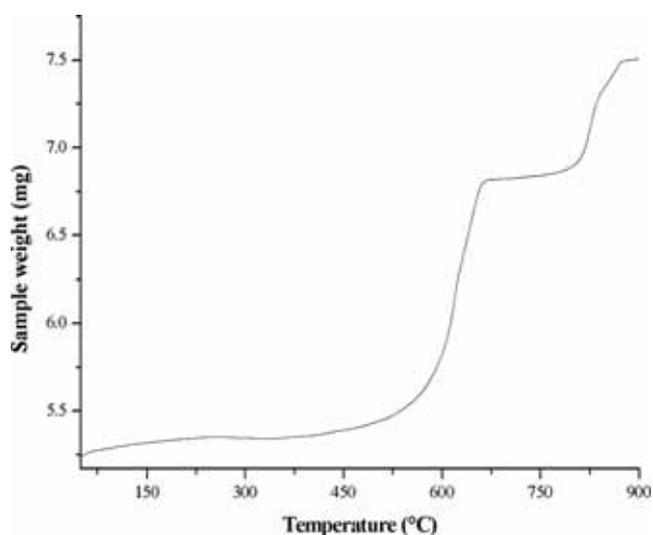
Figure 6. TGA pattern of Ge-NW nanoproducts (50–900°C, O_2, 5°C min^{-1}).

Figure 7. DSC pattern of Ge-NW nanoproducts (100–900°C, O_2, 5°C min^{-1}).

The optical band gap of Ge-NWs has been roughly estimated from the UV–Vis–NIR spectrum detected at photon energies between 0.5 and 7 eV, by applying the common Tauc's procedure for amorphous and quasi-crystalline semiconductors [40–42]. It results of about 0.67 eV, near to that of crystalline Ge [43]. The extrapolated result from experimental spectra can be determined by both the complete NW dehydrogenation and the actual structural arrangement of the materials [33,44].

The electrical measurements applied on substrate-deposited Ge-NWs provide a resistivity value of $1.75 \times 10^{-1}\Omega$ m, that is diagnostically related to semi-conductive electrical properties, supporting the spectroscopic characterization.

Application of the X-ray CVD/thermal treatment combined protocol is required to obtain the high yields and purity of the deposited products. Indeed, a test synthesis replying all the applied experimental conditions, with exclusion of the supporting XRD of gaseous GeH$_4$ precursor, afforded lesser extents of products, especially on the lower surface of quartz substrate, where the bulk concentration of Ge-NW materials is observed. Conversely, the specific deposition route stimulated by X-ray CVD irradiation of reactants without an assisting thermal process, in the metal reactor, produced an amorphous hydrogenated Ge powder (spherical aggregates), in which NWs features are actually absent, as in reported X-ray CVD experiments in glass reactors [32,33]. It can be concluded that, in the experimental combined set-up, no NWs formation mechanism operates at room temperature.

In the comprehensive context of the reaction mechanisms, it is possible that the large amounts of gaseous activated Ge moieties determine the prevalent deposition of amorphous solid-state germanium phases, as experimentally observed in GeH$_4$ irradiation X-ray CVD products [32,33]. By concomitant stimulation of the combined thermal treatment technique, the deposition substrate surface is then activated, and rapid quantitative dehydrogenation with diffuse nucleation
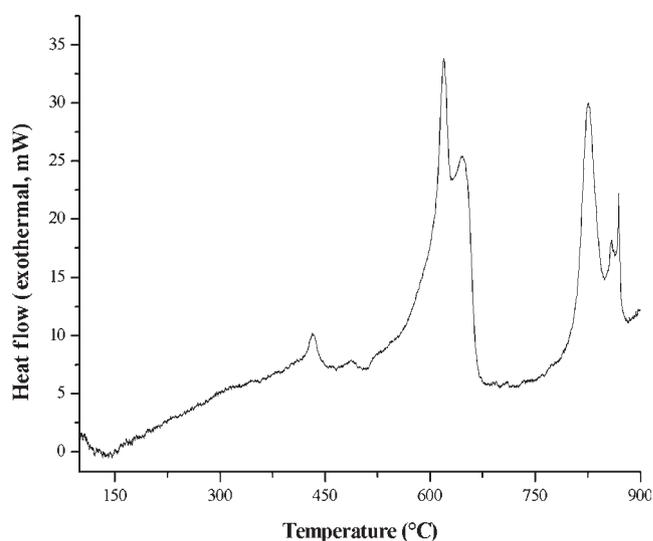
of crystalline Ge-NW structures from highly reactive Ge species can hence occur [35]. The higher deposition rates and radiolytic activation of the growing products above the quartz substrate can stimulate the main formation of an amorphous film. Under the substrate, the higher process temperature and a minor diffusion feedstock flow of activated gaseous reactive Ge moieties can provide the quantitative growth of the high-purity Ge-NW nanomaterials. The experimental lack of added metal catalysis and of metal nanoparticles in Ge-NW products exclude the reported synthetic mechanism of vapour–liquid–solid (VLS) growth process [45–48]. A different base-growth synthetic route [14] can determine the formation of the nanoproducts. The NW nucleation may be promoted by activated sites on the deposition substrate, oriented heteroepitaxy on the quartz surface [16,23], or in a preformed thin-layer germanium amorphous film [21,49]. Indeed, SEM analyses of both surfaces of the quartz deposition substrate observed a thin amorphous layer of germanium film, which can be actually the starting source of nucleation sites of NWs. Noteworthy, similar experimental treatments of X-ray irradiation and thermal annealing have produced germanium crystalline domains from amorphous films [35].

A qualitative possible chemical sequence of the reaction advance on substrate surface is hence tentatively presented in scheme 2.

Noteworthy, the presented deposition growth process does not imply a metal substrate. Although in a base-growth process [14] a support provided by catalytic activity of the adjacent Cu heating platelet might not be excluded as a line of principle (Actually, in separated materials collected from the Cu heating element surface, germanium thinner messy nanotube bundles with lumps were observed quantitatively by SEM-EDAX analysis, expected to form on the metal surface with a base-growth catalysis process [14,48].) [50], similar morphologies of Ge-NW products were formed on both faces of the quartz substrates. The NW nanoproducts

$$\text{X-ray CVD, } \Delta T \text{ (300°C)} \longrightarrow$$

$$GeH_4 \rightarrow {}^*GeH_4 \rightarrow {}^*GeH_{4-x} + (x/2)H_2 \rightarrow \text{a-Ge}_{film} \rightarrow \text{Ge}_{(c)}@\text{a-Ge}_{film} \rightarrow (\text{a-Ge}_{film})\text{-Ge-NWs}$$

Scheme 2. A proposed possible chemical sequence of reaction advance on deposition substrate surface in X-ray CVD thermal synthesis of Ge-NWs (symbol legends, ${}^*GeH_4$: excited species; ${}^*GeH_{4-x}$: dehydrogenated excited species; a-Ge$_{film}$: amorphous germanium thin film; Ge$_{(c)}$@a-Ge$_{film}$: Ge crystal nucleation embedded in amorphous germanium thin film; and (a-Ge$_{film}$)-Ge-NWs: Ge-NWs grown on amorphous germanium thin film).
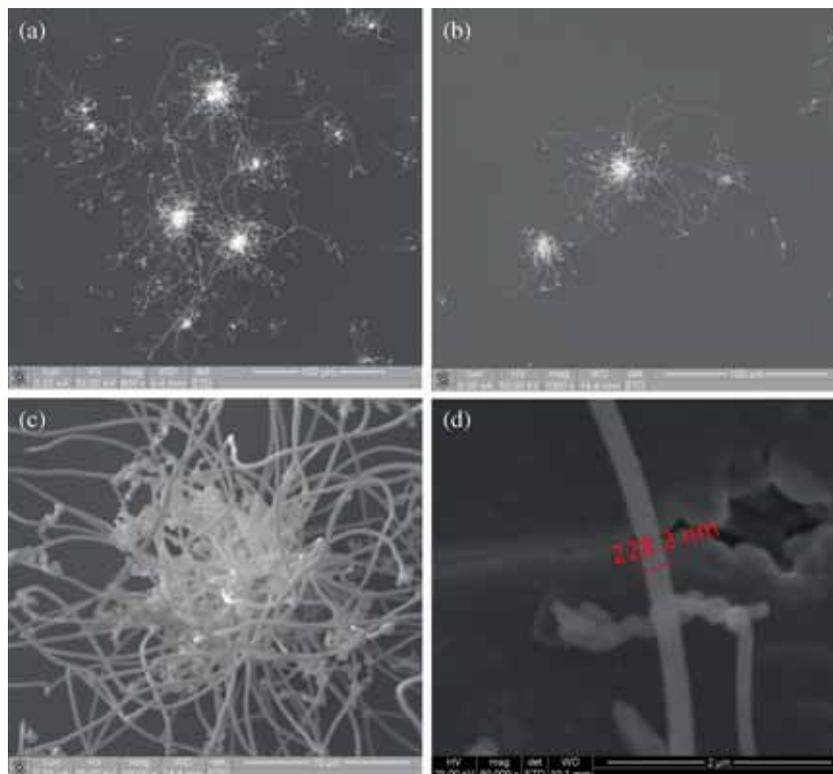

Figure 8. SEM pictures of Ge-NW nanoflowers grown on the upper surface of the quartz substrate (**a–c**). A detail of a nanoflower bundle (**c**). A specific growth-process diameter is reported (**d**).

grown on the higher substrate surface, which is spaced far above from the metal element, induce the opinion of a similar catalyst-free growth mechanism, derived by the combined thermal X-ray CVD deposition on activated surface substrates. The upper side of the substrate, more exposed by the geometrical favourable position to a bulk deposition of activated Ge species, is hereafter covered by a main amorphous Ge layer, presenting specific structural and spectroscopic features characterized herein with XRPD and Raman reported results (figures 4b and 5b), spotted by 'nanoflowers' of Ge-NW bundles. In the reactive perspective, it can be hypothesised that the massive H_2 formation subsequent to GeH_4 dehydrogenation in the adopted experimental conditions may activate the NW nucleation Ge crystalline clusters on the deposited surface films and promote formation of Ge-NW nanoproducts [21,35]. In the NW growth process, peripheral less-ordered Ge may hereafter embed the crystal core source [14]. However, in both surface-deposited NW products, embedded heterogeneous metal nanoparticles

were not observed by EDAX analysis. In a lack of a metal catalyst, different experimental set-up of irradiation time and temperature parameters can provide a different length, diameter and aspect ratio of the nanomaterials. In perspective, it is worth noting here that reduced irradiation times can indeed condition the actual morphology of the nanomaterials, yielding smaller NWs, whereas different deposition temperatures may yield different crystal core sizes. A suggestive set of SEM micrographs of Ge-NWs bundle nanoflowers, embedded in the bulk amorphous Ge phase of the upper substrate surface, is depicted in figure 8a–d. NW lengths of up to 100 micrometers are observed (with a length/diameter aspect ratio near to 500 : 1). Specific Ge-NW diameters in nanoflowers (with average diameter of about 20 μm, containing hundreds of NW filaments) have been measured (figure 8d). By comparison of figures 1 and 8, a NW knots density of about 3–5 units per 100 μm^2 is observed on the higher surface of the deposition substrate [51], while on the lower surface a quantitative NW bundle growth is produced. However,
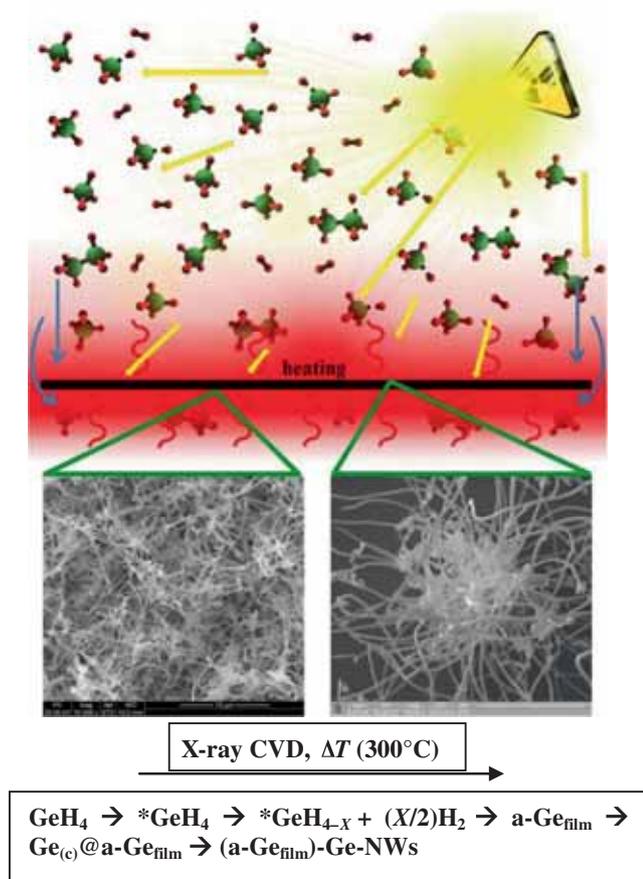
$$GeH_4 \rightarrow {}^*GeH_4 \rightarrow {}^*GeH_{4-X} + (X/2)H_2 \rightarrow a\text{-}Ge_{film} \rightarrow Ge_{(c)}@a\text{-}Ge_{film} \rightarrow (a\text{-}Ge_{film})\text{-}Ge\text{-}NWs$$

Figure 9. Graphical scheme of Ge-NWs synthesis experiment with the reaction advance stimulated by the combined X-ray CVD-thermal treatment techniques.

similar diameter lengths to the products deposited on the lower surface of the quartz substrate were observed, presumably for the similar reactive mechanism of X-ray-formed gaseous Ge moieties on both the thermally activated surfaces. A comprehensive graphical scheme of Ge-NWs synthesis with the X-ray CVD-thermal treatment hyphenated experiment is illustrated in figure 9. The presented result items support a germanium NW growth process without a metal catalysis task to assist the nanoproduct formation.

5. Conclusions

In conclusion, germanium nanowires of high purity and high aspect ratio have been synthesised in bulk quantity by a catalyst-free combined application of X-ray radiolysis–CVD and thermal treatment techniques, at low temperatures with straightforward reaction of the GeH_4 gas molecule. The nanoproducts have been deposited on a conventional quartz substrate, without a specific metal catalytic support. Nanowires are provided with very large aspect ratios (ranging from 100 to 500) and crystalline core morphology, with the comprehensive opto-electronic features that determine semiconductivity results. Finally, the presented

innovative combined protocol may provide an improvement of the synthesis yields and purity of designed nanosubstrates and increase the application of the selected deposition targets, to support development of the manifold possible applications of germanium in material manufacturing items, for different nanotechnology perspectives.

References

[1] Kim J, Bedell S W and Sadana D K 2011 *Appl. Phys. Lett.* **98** 082112

[2] Yamamoto K, Yamanaka T, Ueno R, Hirayama K, Yang H G, Wang D and Nakashima H 2012 *Thin Solid Films* **520** 3382

[3] Tsao C Y, Weber J W, Campbell P, Conibeer G, Song D Y and Green M A 2010 *Sol. Energy Mater. Sol. Cells* **94** 1501

[4] Camacho-Aguilera R E, Cai Y, Patel N, Bessette J T, Romagnoli M, Kimerling L C and Michel J 2012 *Opt. Exp.* **20** 11316

[5] Sorianello V, De Iacovo A, Colace L, Fabbri A, Tortora L, Buffagni E and Assanto G 2012 *Appl. Phys. Lett.* **101** 081101

[6] Pillarisetty R 2011 *Nature* **479** 324

[7] Gerung H, Boyle T J, Tribby L J, Bunge S D, Brinker C J and Han S M 2006 *J. Am. Chem. Soc.* **128** 5244

[8] Yu B, Sun X H, Calebotta G A, Dholakia G R and Meyyappan M J 2006 *J. Clust. Sci.* **17** 579

[9] Heath J R and Legoues F K 1993 *Chem. Phys. Lett.* **208** 263

[10] Hanrath T and Korgel B A 2002 *J. Am. Chem. Soc.* **124** 1424

[11] Schonenberger C, Van der Zande B M I, Fokkink L G J, Henny M, Schmid C, Kruger M, Bachtold A, Huber R, Birk H and Staufer U 1997 *J. Phys. Chem. B* **101** 5497

[12] Morales A M and Lieber C M 1998 *Science* **279** 208

[13] Wu Y and Yang P D 2000 *Chem. Mater.* **12** 605

[14] Mathur S, Shen H, Sivakov V and Werner U 2004 *Chem. Mater.* **16** 2449

[15] Li X, Meng G, Xu Q, Kong M, Zhu X, Chu Z and Li A P 2011 *Nano Lett.* **11** 1704

[16] Adhikari H, Marshall A F, Chidsey C E D and McIntyre P C 2006 *Nano Lett.* **6** 318

[17] Koto M, Marshall A F, Goldthorpe I A and McIntyre P C 2010 *Small* **6** 1032

[18] Thombare S V, Marshall A F and McIntyre P C 2012 *J. Appl. Phys.* **112** 054325

[19] Wang D and Dai H 2002 *Angew. Chem. Int. Ed.* **41** 4783

[20] Skukla B, Saito T, Ohmori S, Koshi M, Yumura M and Iijima S 2010 *Chem. Mater.* **22** 6035

[21] Lotty O, Hobbs R, O'Regan C, Hlina J, Marschner C, O'Dwyer C, Petkov N and Holmes J D 2013 *Chem. Mater.* **25** 215

[22] Barrett C A, Geaney H, Gunning R D, Laffir F R and Ryan K M 2011 *Chem. Commun.* **47** 3843

[23] Jagannathan H, Deal M, Nishi Y, Woodruff J, Chidsey C E D and McIntyre P C 2006 *J. Appl. Phys.* **100** 024318

[24] Yan C Y and Lee P S 2009 *J. Phys. Chem. C* **113** 2208

[25] Kumar R R, Yuvaraj D and Rao K N 2010 *Mater. Lett.* **64** 1766

[26] Mullane E, Geaney H and Ryan K M 2012 *Chem. Commun.* **48** 5446

[27] Lu X T, Harris J T, Villareal J E, Chockla A M and Korgel B A 2013 *Chem. Mater.* **25** 2172

[28] O'Regan C, Biswas S, O'Kelly C, Jung S J, Boland J J, Petkov N and Holmes J D 2013 *Chem. Mater.* **25** 3096

[29] Marshall A F, Goldthorpe I A, Adhikari H, Koto M, Wang Y C, Fu L, Olsson E and McIntyre P C 2010 *Nano Lett.* **10** 3302

[30] Ratchford J B, Goldthorpe I A, Sun Y, McIntyre P C, Pianetta P A and Chidsey C E D 2009 *Langmuir* **25** 9473

[31] Woodruff J H, Ratchford J B, Goldthorpe I A, McIntyre P C and Chidsey C E D 2007 *Nano Lett.* **7** 1637

[32] Arrais A, Benzi P, Bottizzo E and Demaria C 2007 *J. Appl. Phys.* **102** 104905

[33] Arrais A, Benzi P, Bottizzo E and Demaria C 2009 *J. Phys. D: Appl. Phys.* **42** 105406

[34] Antoniotti P, Benzi P, Castiglioni M and Volpe P 1999 *Eur. J. Inorg. Chem.* **1999** 323

[35] Demaria C, Benzi P, Arrais A, Bottizzo E, Antoniotti P, Rabezzana R and Operti L 2013 *J. Mater. Sci.* **48** 6357

[36] O'Regan C, Biswas S, Petkov N and Holmes J D 2014 *J. Mater. Chem. C* **2** 14

[37] (a) Cooper A S 1962 *Acta Crystallogr.* **15** 578 in (b) The Crystallographic Open Database (COD) http://www.crystallography.net

[38] Ikeda H, Qi Y, Cagin T, Samwer K, Johnson W L and Goddard W A III 1999 *Phys. Rev. Lett.* **82** 2900

[39] Gupta S, Katiyar R S, Morell G, Weisz S Z and Balberg I 1999 *Appl. Phys. Lett.* **75** 2803

[40] Tauc J 1974 *Amorphous and liquid semiconductors* (ed.) J Tauc (New York: Plenum) p 159

[41] Kumar R T A, Lekha P C, Sundarakannan B and Padiyan D P 2012 *Philos. Mag.* **11** 1422

[42] Benzi P, Bottizzo E and Demaria C 2006 *Chem. Vap. Dep.* **12** 25

[43] Lieten R R, Bustillo K, Smets T, Simoen E, Ager J W, Haller E E and Loquet J P 2012 *Phys. Rev. B* **86** 0352086

[44] Pan R K, Tao H Z, Zang H C, Zhang T J and Zhao X J 2009 *Physica B: Condens. Matter* **404** 3397

[45] Wagner R S and Ellis W C 1964 *Appl. Phys. Lett.* **4** 89

[46] Park W I, Zheng G F, Jiang X C, Tian B Z and Lieber C M 2008 *Nano Lett.* **8** 3004

[47] Adhikari H, Marshall A F, Goldthorpe I A, Chidsey C E D and McIntyre P C 2007 *ACS Nano* **1** 415

[48] Renard C, Boukhicha R, Gardès C, Fossard F, Yam V, Vincent L, Bouchier D, Hajjar S, Bubendorff J L, Garreau G and Pirri C 2012 *Thin Solid Films* **520** 3314

[49] Kelires P C 1998 *Int. J. Mod. Phys. C* **9** 357

[50] Geaney H, Dickinson C, Barrett C A and Ryan K M 2011 *Chem. Mater.* **23** 4838

[51] Dai L, You L P, Duan X F, Lian W C and Qin G G 2004 *J. Cryst. Growth* **267** 538